Trans Indian Inst Met (2019) 72(3):741–749
https://doi.org/10.1007/s12666-018-1526-2

TECHNICAL PAPER

Evaluation of Mechanical Properties and Microstructures of Ultrafine Grain Low-Carbon Steel Processed by Cryorolling and Annealing

Qing Yuan[1] · Guang Xu[1] · Man Liu[1] · Sheng Liu[1] · Hai-jiang Hu[1]

Received: 3 September 2018 / Accepted: 22 November 2018 / Published online: 18 December 2018

Abstract In the present study, low-carbon steel was first evenly cryorolled by 50% reduction at liquid nitrogen temperature (LNT) and then annealed at 400–550 °C for 1800 s. A transmission electron microscope was employed to analyze the microstructures and the tangled dislocations in the processed steel. The presence of Fe_3C particles in the steel was confirmed by X-ray diffraction method, and the mechanical properties were measured by an electronic universal tensile machine. It was found that cryorolling at LNT significantly improved the potentials of refined ferrite grains. Grain refinement at LNT occurred due to the suppression of dynamic recovery during cryorolling, thus resulting in high defect density and abundant nucleation sites for ferrite grains. An average ferrite grain size of 133 nm was observed in the specimen annealed at 450 °C for 1800 s, and its strength increased to 970.2 MPa with a reasonable ductility of 12.34%. The work extended the cryorolling from alloys and austenitic stainless steels to the low-carbon steels and provided a technical support for the fabrication of ultrafine grained low-carbon steel.

Keywords Ultrafine grain · Cryorolling · Annealing · Martensite · Mechanical property

✉ Guang Xu
xuguang@wust.edu.cn

Qing Yuan
yuanqing@wust.edu.cn

Man Liu
liuman@wust.edu.cn

Sheng Liu
liusheng@wust.edu.cn

Hai-jiang Hu
huhaijiang@wust.edu.cn

[1] The State Key Laboratory of Refractories and Metallurgy, Hubei Collaborative Innovation Center for Advanced Steels, Wuhan University of Science and Technology, 947 Heping Avenue, Qingshan District, Wuhan 430081, China

1 Introduction

Ultrafine grain (UFG) materials possess higher strength as compared to other conventional materials; thus, UFG steels manifest significant potentials to replace high-strength alloyed steels and conform to the sustainable development patterns of steel industries. Therefore, the fabrication of UFG steels with a grain size of < 1 μm has become the prevailing research topic [1–4]. Severe plastic deformation methods (SPDs) [5–11] and thermo-mechanically controlled processes (TMCPs) are usually employed to produce ultrafine grains; however, the requirement of large plastic strains is the main drawback of SPD methods. Tsuji et al. [12] first proposed an effective way to produce UFG low-carbon steels through cold rolling of martensite initial microstructure (with an equivalent strain of 0.8) followed by annealing; this method is often called as martensite method. The average size of ultrafine ferrite grains was found as 180 nm, and the obtained UFG steel yielded a tensile strength (TS) of 870 MPa with an elongation of 20%. Bao et al. [13] and Ueji et al. [14] carried out parallel research on cold deformation and annealing of a martensite initial microstructure. Ashrafi et al. [15] reported the successful fabrication of ultrafine ferrite grains through a heavy ambient compression of martensite and subsequent annealing at 550 °C. The average size of ultrafine ferrite grains decreased to 1.8 μm, and the micro-hardness value reached 210 HV. However, it can be concluded that the

refinement degree of ferrite grain through martensite method was limited.

Cryorolling at liquid nitrogen temperature (LNT) is usually performed to produce UFG steels with improved potentials. Shanmugasundaram et al. [16] applied cryorolling and subsequent annealing at temperatures below 200 °C to refine Al–Cu alloy (2219). The microstructure of the alloy was sharply refined; thus, significant improvements were noticed in its TS and ductility. Panigrahi and Jayaganthan [17] prepared UFG Al alloy (6063) through cryorolling, short-annealing, and aging treatment and observed profound enhancements in its TS (286 MPa) and ductility (14%). Rao et al. [18] reported that the TS value of the cryorolled and annealed Al 6061 alloy increased to 388 MPa with 4.5% elongation. Yu et al. [19], Fritsch et al. [20], and Weiss et al. [21] also propounded similar results. Therefore, three main common features in the above-mentioned investigations can be summarized as follows: (1) experimental materials were mainly nonferrous alloys, such as Cu, Al, and Mg, (2) their mechanical properties, such as strength and ductility, were significantly improved through cryorolling and subsequent annealing, and (3) their grain sizes decreased after cryorolling process. Moreover, cryorolling can also be employed to prepare austenitic stainless steels. Single-phase austenite initial microstructures are used before cryorolling at LNT, and deformation-induced martensite microstructures are obtained during cryorolling process.

However, there are few studies concerning the fabrication of UFG low-carbon steel by means of cryorolling method. Less attention is paid on the microstructure evolution and mechanical properties of low-carbon steel cryorolled with a small equivalent strain at LNT. Hence, the purpose of the present work is to extend the tested material from alloys and austenitic stainless steels to the low-carbon steel and explore an effective way to further refine the grains in low-carbon steel. The effect of cryorolling process on the microstructure evolution and mechanical properties in low-carbon steel was investigated. Moreover, the mechanism of grain refinement by cryorolling process was discussed. It is hoped that this research will provide a reliable theoretical basis as well as technical support for the fabrication of ultrafine grained low-carbon steel.

2 Experimental Procedures

A commercial low-carbon steel ingot of composition Fe–0.165C–0.211Si–0.448Mn–0.014P–0.013S–0.002Als (wt%) was procured from a hot strip plant. Specimens with a length of 90 mm, a width of 15 mm, and a thickness of 3 mm were processed to fabricate ultrafine grains. Figure 1 illustrates the required steps of the cryorolling and heat

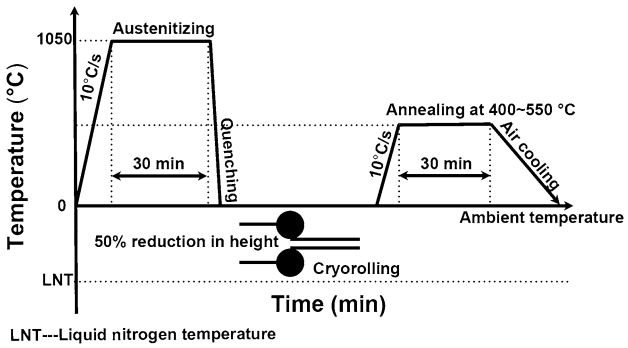

Fig. 1 Schematics of fabrication of ultrafine grain by cryorolling low-carbon steel

treatment process. All specimens were first heated at 1050 °C for 1800 s to ensure the homogeneous austenization and then water-quenched to obtain martensite initial microstructure. All quenched martensite specimens were immersed in liquid nitrogen and held for about 1800 s in order to achieve the LNT, and finally, the cryogenic specimens were quickly cold-rolled on a two-high mill with a roll diameter of 310 to 1.5 mm in five passes. In order to avoid the influences of rolling pass on final microstructures and properties, about 10% deformation was applied to each pass. The cryorolled specimens were then again immersed in liquid nitrogen for 900 s before applying the next 10% deformation. No cracks occurred during the cryorolling process. The total reduction was 50%, namely a 0.8 equivalent strain, which was much smaller as compared to other SPD processes. In order to analyze the microstructures before annealing, room-temperature rolling experiment was conducted under 50% reduction and five passes. After cryorolling, specimens were annealed at 400–550 °C for 1800 s followed by air cooling to room temperature (RT). The annealing temperatures were selected by considering the theoretical recrystallization temperature of the tested steel and annealing temperatures for similar steels used by other studies [5, 12]. Annealing time of 1800 s was chosen based on the authors' previous study on annealing treatment of low-carbon steel rolled at room temperature [22].

All specimens were first grounded and polished and then etched with 4 vol% Nital for microstructural characterization. The morphologies of the specimens were analyzed by a Zeiss optical microscope (OM) and a field-emission scanning electron microscope (FE-SEM) with an accelerating voltage of 20 kV. Rolling direction (RD) was considered as the observation direction. In addition, the distributions of dislocations after rolling were observed by a JEM-2100F transmission electron microscope (TEM). Moreover, X-ray diffraction (XRD) technique was adopted to confirm the precipitates. Grain size was measured by means of the mean linear intercept method (MLIM), and

five graphs were measured in order to improve measurement accuracy. Tensile tests of the annealed specimens were performed on a UTM-4503 electronic universal tensile machine at RT. The crosshead was set to 1 mm/min, and the displacement direction was parallel to RD. The gauge size of all tensile specimens was 5 mm (length) × 1.2 mm (width) × 0.6 mm (thickness). Repeated tensile tests were performed for each specimen annealed at various temperatures. Additionally, for comparing the microstructure and mechanical properties between base steel and UFG steel fabricated by cryorolling, tensile test and microstructure observation of the base steel were conducted as well.

3 Results and Discussion

3.1 Microstructure

The initial microstructure of the base steel mainly consists of equiaxed polygon ferrites (F) and irregular-shaped pearlites (P) (Fig. 2). Moreover, two different types of gray levels are observed in ferrite grains due to different crystal orientations and corrosion degrees. The volume fractions of ferrite and pearlite have been measured using Image Pro-plus 6.0 software. Figure 2c, d is achieved by the color aberration function in the software, and the volume fractions of F and P are found as 88.74 ± 5.88% and 11.26 ± 3.41%, respectively. In addition, the average size of ferrite grains is determined to be 22.51 ± 2.11 μm. Three images have been analyzed to improve measurement accuracy, and the average values are considered as the final values.

After quenching, lathy martensites are formed in the experimental low-carbon steel (Fig. 3a). In order to examine the microstructures of the obtained martensite, micro-hardness test is performed on a hardness testing machine under a loading force of 100 g and a loading time of 10 s (Fig. 3b), and the hardness of the martensites is found to be 475.11 Hv, which complies with the microstructure reported by Ueji et al. [14] and Okitsu et al. [23]. Hence, it can be inferred that martensite starting microstructure facilitates the grain refinement process for the following reasons. Firstly, carbides (Fe_3C) evenly precipitate in ferrite grain boundaries due to the oversaturated solid solution of carbon in martensite and prevent any further grain growth by pinning effect. Secondly, the misorientations in lathy martensites further subdivide the annealing structure. Furthermore, martensites manifest high dislocation density and increase the distortion energy during rolling and, consequently, facilitate the development of ultrafine grains during annealing [23, 24].

It has already been proved that martensite microstructures with low-carbon contents can be cold-rolled to 50–

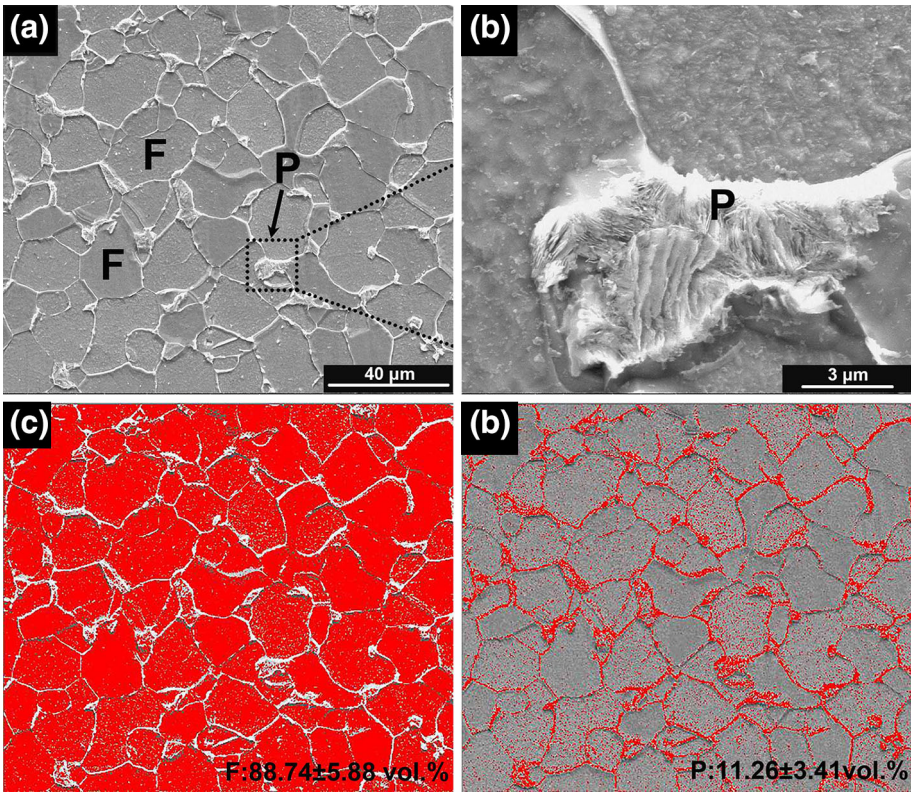

Fig. 2 Initial microstructure of low-carbon steel **a** F + P, **b** P, **c** measurement of F content and **d** measurement of P content

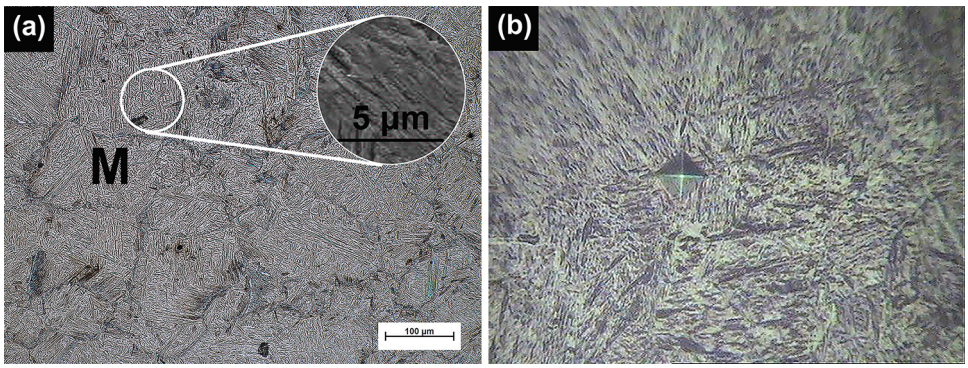

Fig. 3 Martensite initial microstructure (**a**) and **b** its hardness

75% reduction [5–7, 12, 14]. Cryorolling lath martensite to 50% reduction at LNT has also been smoothly realized in the present study. As the carbon content is low, the microhardness of immersed martensite is tested to be 545.28 HV, which is within the required rolling load of a two-high mill. In addition, multi-pass small reductions are applied to avoid any large stress and crack. Figure 4 displays the microstructures of martensites with 50% reduction at LNT. It is observed that most of the lathy martensites are elongated along RD. Three different substructures are identified in the obtained martensites: (1) lamellar dislocation cell (LDC) with flowing wavy morphology along RD, (2) an irregularly bent lamellar structure (IBL), and (3) kinked lath (KL) structure. It is found that LDC and IBL substructures mainly consist of high-angle grain boundaries [12, 23, 25]. Generally, LDC substructures are formed from severe plastic deformation; however, in the present experiment, LDC substructures are obtained by a relatively small equivalent strain of 0.8. Further, in kinked lath (KL) structure, lathy martensites are kinked by shear bands. Figure 4b exhibits the percentages of these substructures in lathy martensites with 50% reduction at LNT. It is evident that the LDC substructure occupies the largest area (64.82%), whereas the IBL structure possesses the smallest area (9.92%). Okitsu et al. [23] argued that 50% LDC substructure can be obtained by 50% reduction and 100% LDC substructure can be achieved by almost 70% reduction at RT. Therefore, it certifies that more LDC substructure is formed from cryorolling martensite with the same reduction, promoting nucleation of recrystallization grain due to the increase in misorientation. The main reason is that, the deformation resistance significantly increases at LNT resulting in the bigger required deforming force under a constant reduction than that rolled at RT. Hence, the deformation trend of blocky martensite is unanimous and shows more flowing wavy morphology at LNT. Equation (1) depicts the relationship between adiabatic temperature rise (ΔT) and strain (ε).

$$\int_{T_0}^{T_0+\Delta T} \rho C \mathrm{d}T = \int_{\varepsilon_0}^{\varepsilon_0+\Delta\varepsilon} \sigma \mathrm{d}\varepsilon \Rightarrow \Delta T = \frac{\bar{\sigma}\Delta\varepsilon}{\rho C}, \tag{1}$$

where ρ denotes material density, σ signifies true stress, C expresses specific heating, $\Delta\varepsilon$ depicts strain interval, and $\bar{\sigma}$ is the mean stress. It is clear that ΔT increases with an increase in ε. However, in the current experiment,

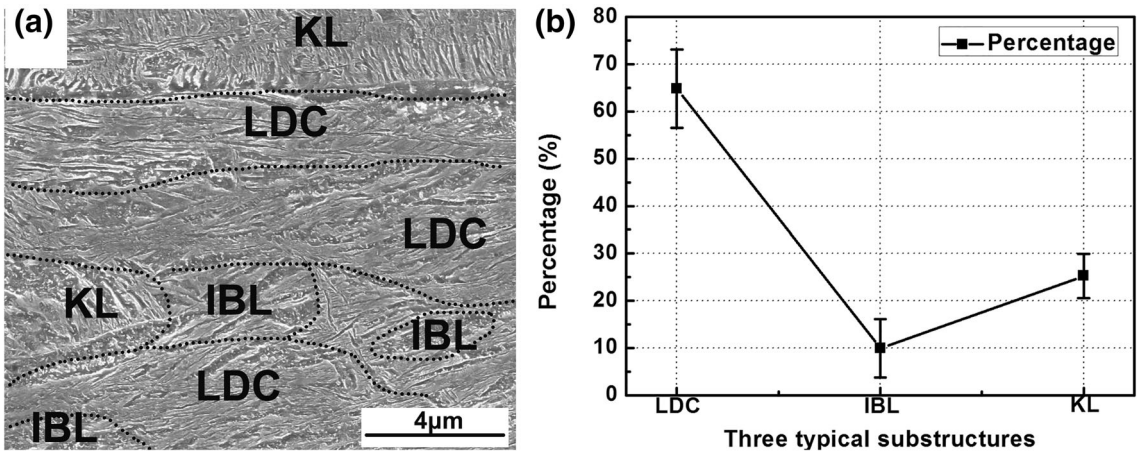

Fig. 4 Deformed martensite microstructure distinguished by three typical substructures (**a**) and **b** percentage of different substructures

ΔT resulting from the rolling deformation is repressed at LNT. Atomic diffusion and dynamic recovery are powerfully repressed at LNT; thus, atoms' vacancies and defects are continuously amassed, and consequently, these surviving defects transform into substructures.

The TEM micrographs in Fig. 5 compare the dislocation distributions after rolling at LNT and RT. It is observed that lathy martensites are found to be refined in the cryorolled specimen at LNT (Fig. 5c). The refined lathy martensites are ascribed to the greater deformation resistance at LNT. Moreover, the dislocation density of cryorolled specimen (Fig. 5d) is much higher than that of the specimen cold-rolled at RT. In conclusion, it is easier for the deformation dislocation defects to persist and accumulate as the repression of dynamic recovery at LNT.

The cryorolled specimens are first annealed at 400–550 °C for 1800 s and then air-cooled to ambient temperature. The microstructures of recrystallized ferrite grains at 400–550 °C are illustrated in Fig. 6. A small amount of elongated recrystallized ferrite grains is noticed in the specimen annealed at 400 °C (Fig. 6a); hence, it can be inferred that the recrystallization process starts at 400 °C. In the investigations of Tsuji and Maki [25] and author's previous study [22], the recrystallization temperature has been found to be about 500 °C for the specimens cold-rolled at room temperature. According to Eq. (2):

$$T_{\mathrm{R}} = (0.35 \sim 0.4)T_{\mathrm{M}}, \tag{2}$$

where T_{R} is the theoretical temperature of recrystallization and T_{M} is the melting point of steel. Therefore, the lowest theoretical temperature of recrystallization is nearly 550 °C. In the present study, the recrystallization temperature is not only obviously smaller than theoretical recrystallization temperature of 550 °C, but also lower than that in the specimens deformed at room temperature. This may be attributed to the suppression of dynamic recovery and dynamic recrystallization during cryorolling. The dislocation and deformation defects in the cryorolled samples are much more than in the samples rolled at RT, resulting in a lower starting temperature of recrystallization.

Figure 6b exhibits the recrystallization structure of the specimen annealed at 450 °C for 1800 s. It is noticeable that the recrystallized microstructure consists of equiaxed ultrafine ferrites and irregular carbide particles, and the grain boundaries of ultrafine ferrites are distinct. Similar microstructures are also reported by Hosseini et al. [26] and Wang et al. [27]. However, the temperature for complete

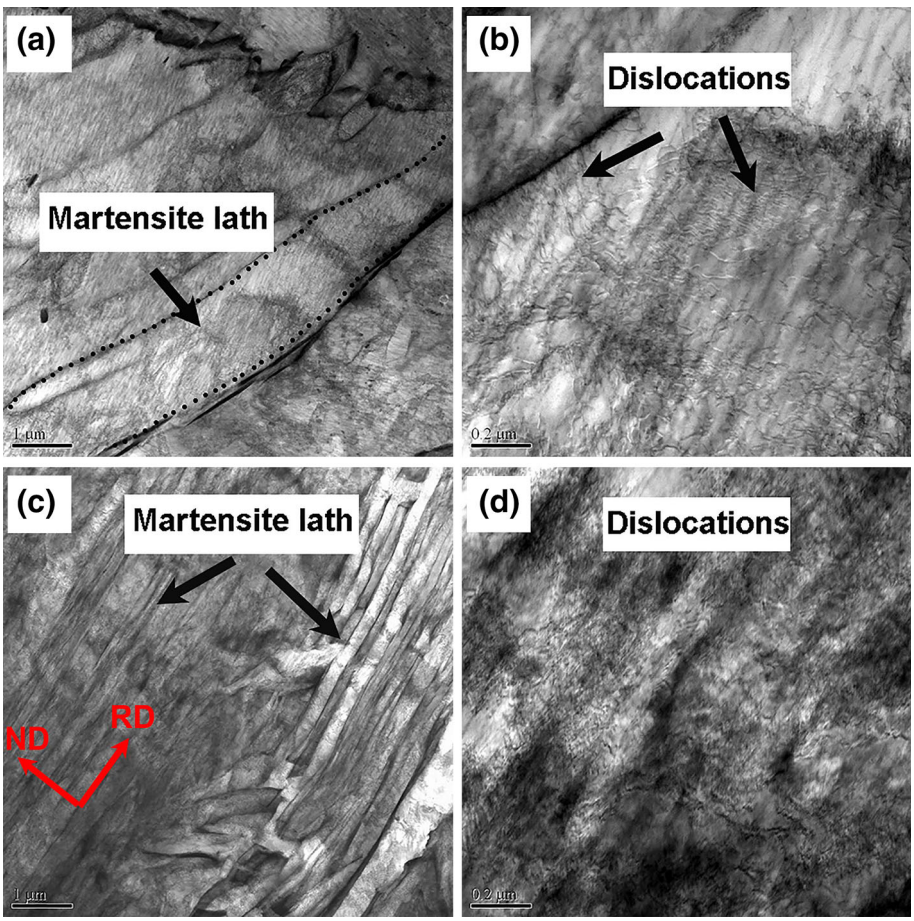

Fig. 5 TEM micrographs showing the morphology of as-rolled martensite and dislocation: **a**, **b** specimen rolled at room temperature; **c**, **d** specimen rolled at LNT

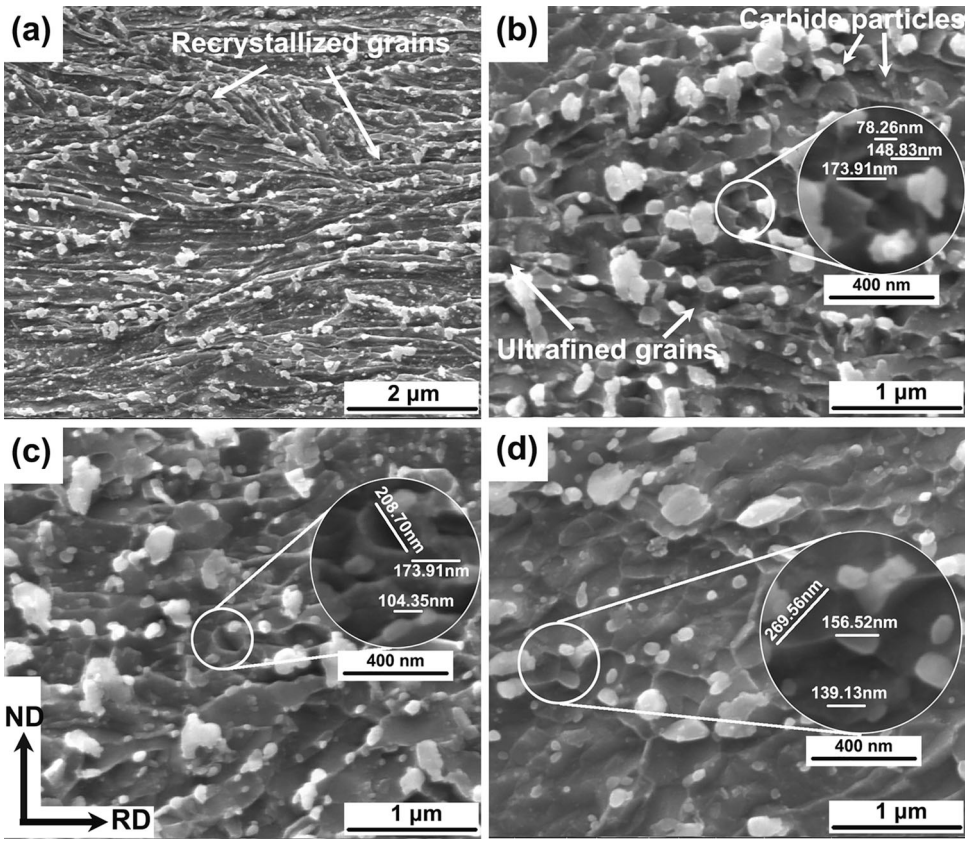

Fig. 6 Microstructures at different annealing temperatures: **a** 400 °C, **b** 450 °C, **c** 500 °C, **d** 550 °C

recrystallization significantly decreases as compared to the specimens deformed at RT.

Figure 7 displays the XRD result of Fe_3C particles. The Fe_3C particle precipitations are formed from the oversaturated solid solution of carbon in martensite. The volume fraction of Fe_3C has been found to be 7–10% in tested 0.165%C steel. In author's previous study [22] and other's results [5, 6, 14, 28] for room-temperature rolling, the amount of Fe_3C particles is found to be about 3.8–7.0%. The size and amount of Fe_3C particles formed in the cryorolled specimen are relatively larger. This is because there are larger dislocation density and distortion energy in specimen cryorolled at LNT, making carbon atoms in an unstable state, resulting in the easy migration of carbon atoms and the coarsening of cementite.

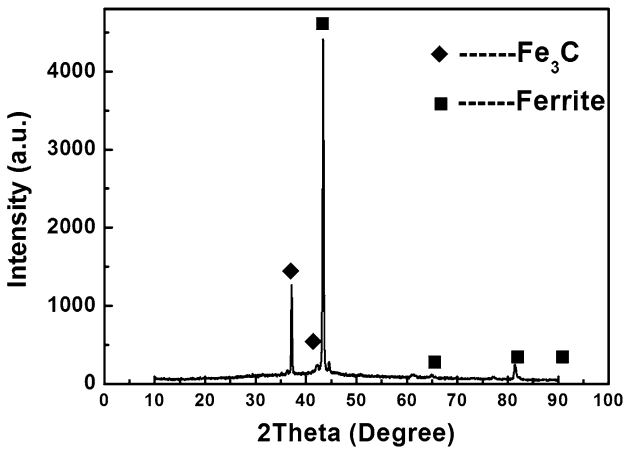

Fig. 7 XRD pattern displaying dominant diffraction peaks of ferrite and diffraction peaks of Fe_3C

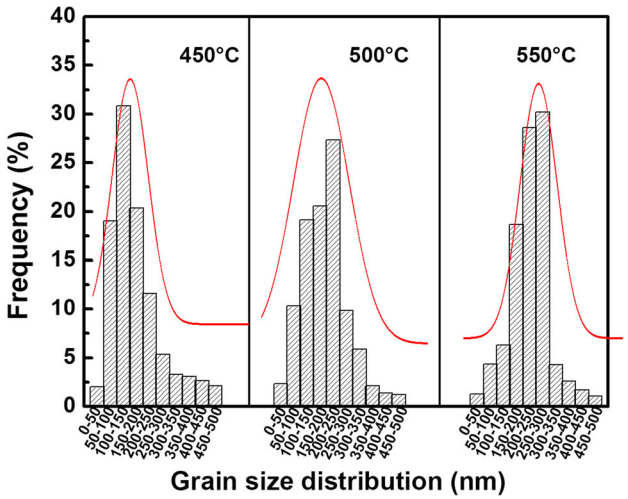

Fig. 8 Grain dimension distribution at different annealing temperatures

The distributions of ferrite grains at different annealing temperatures are displayed in Fig. 8. The fitting lines reveal that the distributions of ferrite grains conform to the Gaussian distribution. The mean ferrite sizes of the specimens annealed at 450 °C, 500 °C, and 550 °C are calculated as 133.4 nm, 161.2 nm, and 187.3 nm, respectively; therefore, it can be found that the mean dimensions of ferrite grains increase with the increasing annealing temperatures. Further, the ranges of mean dimension of the specimens annealed at 450 °C, 500 °C, and 550 °C are found to be 50–250 nm, 100–300 nm, and 150–350 nm, respectively. The dimensions of ultrafine equiaxed ferrite grains at LNT sharply reduces as compared to the reported results in the previous literature [5, 12, 13, 27, 29]. Therefore, it can be posited that ferrite grains get further refined at LNT due to the following reasons. Firstly, the dynamic recovery process including the cross-slips of screw dislocations and the climbs of edge dislocations is restrained at LNT, thus resulting in a higher dislocation density. Hence, affluent nucleation sites for the ferrite grains are introduced by the dislocations. Secondly, the thickness of lathy martensite get significantly reduced at LNT (Fig. 5c). Thirdly, the lower recrystallization temperature facilitates the development of ultrafine ferrite grains through cryorolling deformation.

3.2 Mechanical Property

The tensile strength and the elongation of base steel are 435 MPa and 29.3%, respectively. The stress–strain curves of the specimens cryorolled and annealed at 450–550 °C for 1800 s are presented in Fig. 9. The 50% cryorolled specimen manifestes the maximum TS of 1389.5 MPa; however, its necking happens at an early stage of the tensile experiment; thus, the total elongation of the as-cryorolled specimen is found to be less than 6%. Furthermore, the tensile fracture of the as-cryorolled specimen is flat without any distortion. The high strength and low elongation can be attributed to the poor work-hardening behavior of cryorolling specimen. Furthermore, the value of TS decreases with the increasing annealing temperatures. The specimen annealed at 450 °C for 1800 s manifests an excellent strength of 970.2 MPa and a decent elongation which can meet most engineering requirements. The well combination of strength and elongation in the specimen annealed at 450 °C is profited by much finer grain dimension. The tensile strengths and the elongations of the specimens annealed at 500 °C and 550 °C for 1800 s are 875.3 MPa and 16.48%, and 740.3 MPa and 17.53%, respectively. Compared with the base steel, the weak elongation in ultrafine grains can be charged upon its poor work hardening ability induced by size effect and poor capacity to accumulate defects in tiny grains. In addition, ductile fracture patterns with apparent shearing sections are observed in annealed steel specimens.

Figure 10 summarizes the results of the present work and other previous investigations. Zone I represents high-strength steels with relatively poor elongations (< 10%), zone II refers to steels with good elongation and comparatively lower strength, and steels in zone III manifest an optimal balance between strength and elongation. Therefore, the specimen cryorolled and annealed at 450 °C for 1800 s possesses an excellent strength with an adequate ductility.

The differences between the mean grains and mechanical properties in different investigations in Fig. 10 may be attributed to the following reasons. The first one is the initial microstructure. Ferrite and martensite, as the dual-phase structure, are generally utilized to develop mixed grains (with a combination of coarse and fine grains) in

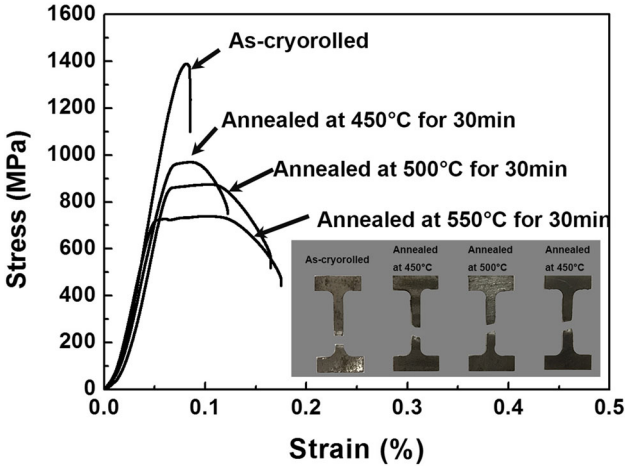

Fig. 9 Stress–strain curves of specimens cryorolled and annealed at different temperatures

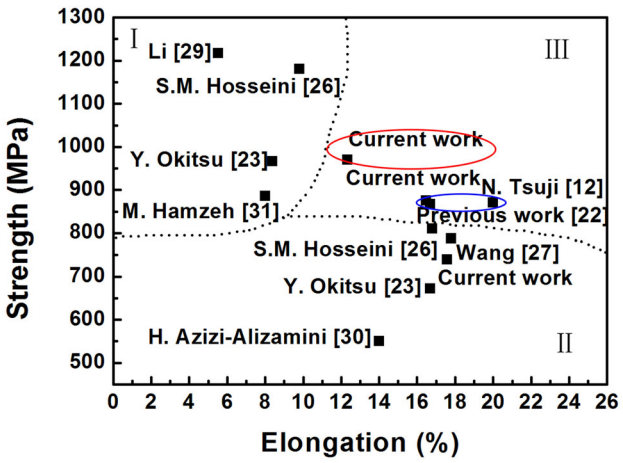

Fig. 10 Schematic diagram of strength and elongation in ultrafine grained steels

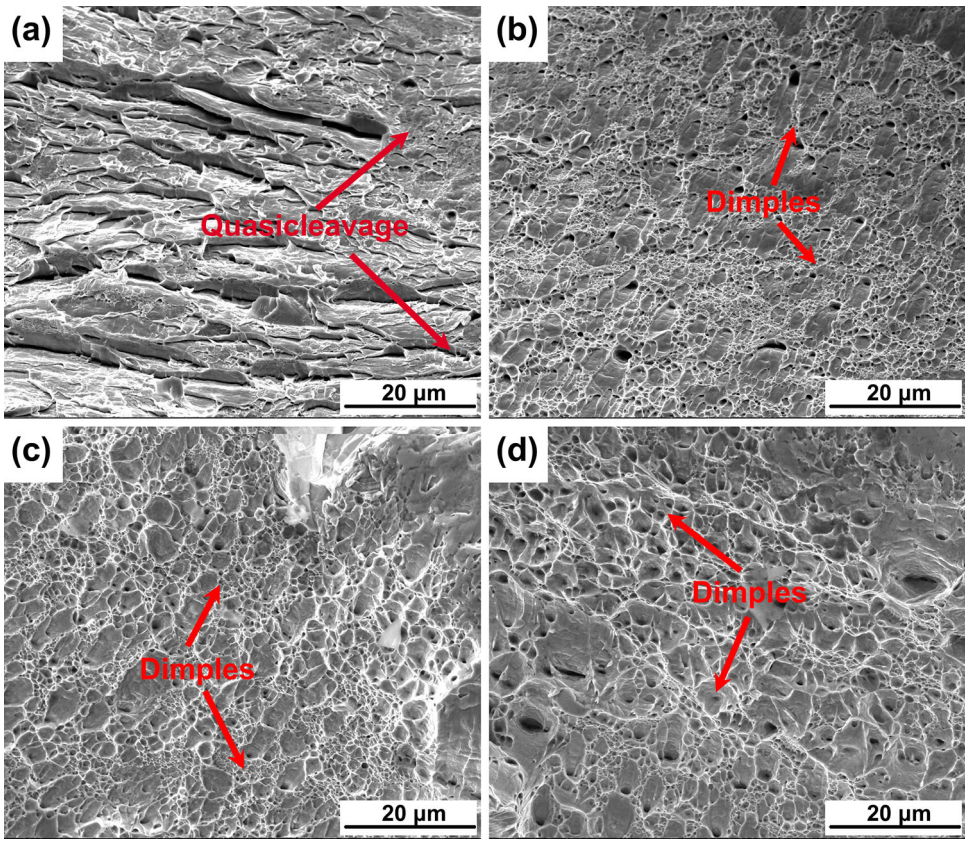

Fig. 11 Tensile fractures of specimens cryorolled and annealed at different temperatures

low-carbon steels [26, 27, 30]. Coarse grains offer good elongations, whereas fine grains yield an improved strength. However, the strength is sacrificed to some extent due to the existence of coarse grains. In addition, bainite initial microstructure also manifests a considerable potential for grain refinement [31]; however, the refinement of ferrite grains is restricted due to relatively small defect density in bainite lamella. Martensite is regarded as the ideal initial microstructure for the production of ultrafine grains in carbon steels [12, 13, 15, 22–25, 29]. The grain dimension can be decreased to nanoscale. The second reason is the different reduction amounts. A larger reduction generates finer grains, thus resulting in higher strengths and lower elongations in deformed steels. Further, annealing conditions (temperature and time) can control the recovery and the recrystallization of deformed samples. It is generally found that grain dimensions increase with the increasing annealing temperatures and time. Lastly, deformation temperature is another key factor. Other investigations utilizes room-temperature deformation or warm deformation, whereas cryorolling at LNT is used in the present work.

It is evident from Fig. 10 that the specimens cryorolled at LNT and annealed at a suitable temperature manifests excellent strengths with adequate ductility. It is clear that cryorolled specimens with 50% reduction manifests high strengths and excellent elongations at a relatively low-annealing temperature (450 °C). As compared to cold-rolled specimens at RT, the average ferrite grain size of cryorolled specimens is found to be 133 nm. In comparison with the results reported by Tsuji et al. [12], smaller ferrite grains with improved strengths are obtained in the present study; however, their elongations are much smaller. The decrease in elongation can be attributed to the presence of large Fe_3C particles in 0.165 wt% C steel.

3.3 Fracture Morphology

Figure 11 displays the fracture surfaces of as-cryorolled and annealed steel specimens. A large amount of legible quasi-cleavage is observed in the as-cryorolled specimen (Fig. 11a), while dimples are found in the annealed specimens. Moreover, dimple size increases with the increasing annealing temperatures, thus resulting in an improved ductility at higher annealing temperatures.

In summary, cryorolling of martensite starting microstructure at LNT to further refine the grains in low-carbon steel is proposed in the present study. The strength and the elongation of the ultrafine low-carbon steel (prepared by cryorolling and annealing) have been calculated as 970.2 MPa and 12.34%, respectively. The dimension of ferrite grains is reduced to about 133 nm as well as an

increased strength of 535.2 MPa with reasonable sacrifice in elongation compared with the base steel. Dynamic recovery and dynamic recrystallization may happen during rolling. But, dynamic recrystallization could not occur during cryorolling due to very low temperature. Even the dynamic recovery is suppressed as well. Therefore, the dislocation and deformation defects continue to accumulate, resulting in a higher level of accumulated dislocations than that achievable at RT. The high density of dislocations and distortion energy including stacking fault energy stored during processing at LNT provide copious nucleation sites during recrystallization, causing the lower starting and finishing temperatures of recrystallization. The intrinsic mechanism of grain refinement is the restrain of the dynamic recovery during cryorolling, thus resulting in a high defect density, larger driving force, and abundant nucleation sites for the ferrite grain formation.

4 Conclusions

A new method of cryorolling martensite starting microstructure by multi-pass small reduction and following annealing to fabricate UFG low-carbon steel has been introduced in the present study. Results indicate that cryorolling martensite starting microstructure at LNT and subsequent annealing provide a potential in fabricating UFG steel with finer ferrite grain. The grain refinement mechanism of cryorolling at LNT is the suppression of the dynamic recovery during cryorolling, resulting in high defect density and abundant nucleation sites for the ferrite grains formation. The average size of ferrite grains has been refined to about 133 nm. The strength and elongation of the specimen annealed at 450 °C for 1800 s are 970 MPa and 12.34%, respectively. The work extends the cryorolling from alloys and austenitic stainless steels to the low-carbon steels. The results provide a reliable theoretical basis for the preparation of ultrafine grained low-carbon steel.

Acknowledgements The authors gratefully acknowledge the financial supports from The Major Projects of Technology Innovation of Hubei Province (2017AAA116), the National Natural Science Foundation of China (NSFC) (Nos. 51874216 and 51704217), and Hebei Joint Research Fund for Iron and Steel (E2018318013).

References

1. Lu K, *Science* **345** (2014)1455.
2. Wang B F, Sun J Y, Zou J D, Vincent S, and Li J, *J Cent South Univ* **22** (2015) 3698.
3. Matsybara K, Miyahara Y, Horita Z, and Langdon T G, *Acta Mater* **51** (2003) 3073.
4. Shin D H, Kim B C, Park K, and Kim Y S, *Acta Mater* **48** (2000) 2247.
5. Tsuji N, Shiotsuki K, and Saito Y, *Mater Trans JIM* **40** (1999) 765.
6. Tsuji N, Ueji R, and Saito Y, *Mater Jpn* **39** (2000) 961. (in Japanese)
7. Saito Y, Utsunomiya H, Tsuji N, and Sakai T, *Acta Mater* **47** (1999) 579.
8. Belyakov A, Sakika Y, Hara T, Kimura Y, and Tsuzaki K, *Metall Mater Trans A* **34** (2003) 131.
9. Takaki S, Kawasaki K, and Kimura Y, in *Ultrafine grained materials*, (eds) Mishra R S, The Minerals, Metals & Materials Society (TMS), Warrendale (2000).
10. Valiev R Z, Ivanisenko Y, Rauch E F, and Baudelet B, *J Mater Sci* **47** (2012) 7789.
11. Horita Z, Smith D, Furukwa M, Nnemoto M, Valiev R Z, and Langdon T G, *J Mater Res* **11** (1996) 1880.
12. Tsuji N, Ueji R, Minamino Y, and Saito Y, *Scripta Mater* **46** (2002) 305.
13. Bao Y Z, Adachi Y, Toomine Y, Xu P G, Suzuki T, and Tomota Y, *Scripta Mater* **53** (2005) 1471.
14. Ueji R, Tsuji N, Minamino Y, and Koizumi Y, *Acta Mater* **50** (2002) 4177.
15. Ashrafi H, and Najafizadeh A, *Trans Indian Inst Met* **8** (2016) 1467.
16. Shanmugasundaram T, Murty B S, and Sarma V S, *Scripta Mater* **54** (2006) 2013.
17. Panigrahi S K, and Jayaganthan R, *Metall Mater Trans A* **41A** (2010) 2675.
18. Rao P N, Singh D, and Jayaganthan R, *Mater Design* **56** (2014) 97.
19. Yu H L, Tieu A K, Lu C, Liu X H, Godbole A, and Kong C, *Mater Sci Eng A* **568** (2013) 212.
20. Fritsch S, Hunger S, Scholze M, Hockauf M, and Wagner M F X, *Mater Sci Eng Tech* **42** (2011) 573.
21. Weiss M, Taylor A S, Hodgson P D, and Stanford N, *Acta Mater* **61** (2013) 5278.
22. Yuan Q, Xu G, Tian J Y, and Liang W C, *Arab J Sci Eng* **42** (2017) 4771.
23. Okitsu Y, Takatab N, and Tsuji N, *Scripta Mater* **60** (2009) 76.
24. Tian J Y, Xu G, Liang W C, and Yuan Q, *Metallogr Microstruct Anal* **6** (2017) 233.
25. Tsuji N, and Maki T, *Scripta Mater* **60** (2009) 1044.
26. Hosseini S M, Alishahi M, Najafizadeh A, and Kermanpur A, *Mater Lett* **74** (2012) 206.
27. Wang T S, Zhang F C, Zhang, M and Lv B, *Metall Mater Trans A* **485** (2008) 456.
28. Ueji R, Tsuji N, Minamino Y, and Koizumi Y, *Sci Technol Adv Mat* **5** (2004) 153.
29. Li X, Jing T F, Lu M M, and Zhang J W, *J Mater Eng Perform* **21** (2012) 1496.
30. Alizamini H A, Militzer M, and Poole W J, *Scripta Mater* **57** (2007) 1065.
31. Hamzeh M, Kermanpur A, and Najafizadeh A, *Mater Sci Eng A* **593** (2014) 24.